

# Conductive resilient graphene aerogel via magnesiothermic reduction of graphene oxide assemblies

Huang Tang<sup>1</sup>, Peibo Gao<sup>1</sup>, Zhihao Bao<sup>1</sup> (✉), Bin Zhou<sup>1</sup>, Jun Shen<sup>1</sup>, Yongfeng Mei<sup>2</sup>, and Guangming Wu<sup>1</sup> (✉)

<sup>1</sup> Shanghai Key Laboratory of Special Artificial Microstructure Materials and Technology, School of Physics Science and Engineering, Tongji University, 1239 Siping Road, Shanghai 200092, China

<sup>2</sup> Department of Materials Science and Engineering, Fudan University, 220 Handan Road, Shanghai 200433, China

**Received:** 26 October 2014

**Revised:** 27 November 2014

**Accepted:** 30 November 2014

© Tsinghua University Press and Springer-Verlag Berlin Heidelberg 2015

## KEYWORDS

graphene aerogel, magnesiothermic reduction, conductivity, mechanical properties

## ABSTRACT

Graphene aerogels are desirable for energy storage and conversion, as catalysis supports, and as adsorbents for environmental remediation. To produce graphene aerogels with low density, while maintaining high electrical conductivity and strong mechanic performance, we synthesized graphene aerogels by the magnesiothermic reduction of a freeze-dried graphene oxide (GO) self-assembly and subsequent etching of the formed MgO in acid solution. The reduced graphene oxide (rGO) aerogel samples exhibited densities as low as  $1.1 \text{ mg}\cdot\text{cm}^{-3}$ . The rGO aerogel was very resilient, exhibiting full recovery even after being compressed by strains of up to 80%; its elastic modulus ( $E$ ) scaled with density ( $\rho$ ) as  $E\sim\rho^2$ . The rGO aerogels also exhibited high conductivities (e.g.,  $27.7 \text{ S}\cdot\text{m}^{-1}$  at  $3.6 \text{ mg}\cdot\text{cm}^{-3}$ ) and outperformed many rGO aerogels fabricated by other reduction processes. Such outstanding properties were ascribed to the microstructures inherited from the freeze-dried GO self-assembly and the magnesiothermic reduction process.

## 1 Introduction

Graphenes are layers of  $\text{sp}^2$  bonded carbon atoms with a hexagonal arrangement, including single layer, few-layer, and multilayer graphenes [1–3]. They exhibit outstanding intrinsic mechanical, physical, and chemical properties [4–6]. For example, graphene has an ultra-high modulus (1 TPa) and electron mobility ( $2.5 \times 10^5 \text{ cm}^2\cdot\text{V}^{-1}\cdot\text{s}^{-1}$ ) [7, 8]. However, the restacking and poor dispersion of graphene nanosheets sometimes limits their viability in practical applications [7]. To

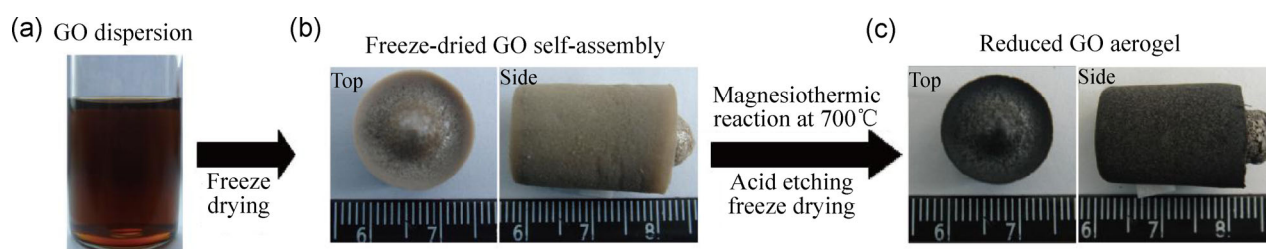
overcome this, three-dimensional (3D) networks, or graphene aerogels (sponges), have been designed and fabricated for use in a variety of applications such as energy storage and conversion, catalysis supports, and adsorbents for environmental remediation [9–16]. The challenge in synthesizing graphene aerogels lies in achieving a low density while maintaining the high conductivity and strong mechanical properties inherited from graphene nanosheets. So far, the most common method for synthesizing such aerogels is the reduction of graphene oxide (GO), the most popular

Address correspondence to Zhihao Bao, zbao@tongji.edu.cn; Guangming Wu, wugm@tongji.edu.cn

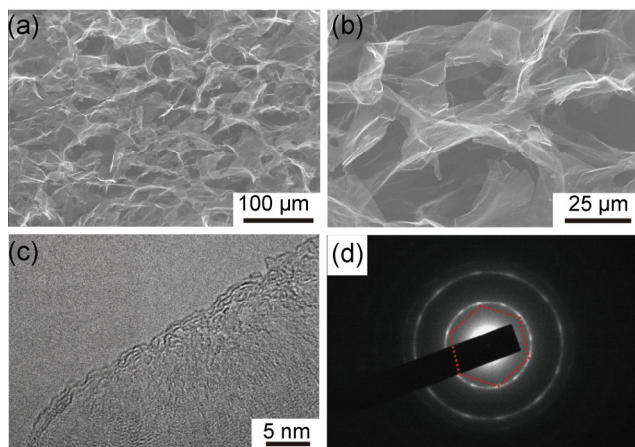
precursor of graphenes [13, 14, 17–21]. Graphene aerogels were formed either by reduction of a GO assembly from freeze/critical-point drying or by in-situ self-assembly during the reduction of GO nanosheets, with reducing agents such as hydrazine and ascorbic acid [10, 13, 17]. Due to the nature of low-temperature reduction using these reducing agents, such graphene aerogels exhibited a low C/O ratio and moderate conductivity and mechanical properties, although low density was achieved [17]. High-temperature reduction of GO could achieve a higher C/O ratio; however, it has not proven to be feasible for the reduction of a GO assembly in general because of the release of gas during heating, which results in a broken structure [22]. To obtain graphenes with high conductivity ( $87\text{S}\cdot\text{m}^{-1}$  at  $10\text{mg}\cdot\text{cm}^{-3}$ ), GO nanosheets had to be cross-linked with resorcinol-formaldehyde resin before being pyrolyzed in  $\text{N}_2$  at  $1,050\text{ }^\circ\text{C}$  [19]. Recently, Mg vapor was found to act as a powerful agent for reducing silicon oxide preforms into silicon replicas while preserving their microstructures [23, 24]. However, to the best of our knowledge, Mg vapor as a reducing agent has not been used on GO self-assemblies. Herein, we report on a process involving a magnesiothermic reaction at  $700\text{ }^\circ\text{C}$  to reduce freeze-dried GO self-assemblies into graphene aerogels with a densities as low as  $1.1\text{ mg}\cdot\text{cm}^{-3}$ . The reduced graphene oxide (rGO) aerogels also exhibited high conductivities (e.g.,  $27.7\text{ S}\cdot\text{m}^{-1}$  at  $3.6\text{ mg}\cdot\text{cm}^{-3}$ ) and good mechanical properties (e.g., the maximum stress level was only reduced by 20% after 1,000 compression cycles). In other words, their performance was superior to that of graphene aerogels fabricated by other reduction processes.

Figure 1 illustrates the synthesis process of the rGO aerogel. GO nanosheets (Fig. S1) with a uniform thickness of  $\sim 1.0\text{ nm}$  were synthesized via a modified

Hummer's method [25, 26]. Their aqueous dispersion (Fig. 1(a)) was then freeze-dried into a cylindrical, grey-colored GO self-assembly (Fig. 1(b)) with a density of  $4.5\text{ mg}\cdot\text{cm}^{-3}$ . After magnesiothermic reduction at  $700\text{ }^\circ\text{C}$  for 5 h, and subsequent acid etching and freeze-drying, the self-assembly's color turned to black, while preserving the cylindrical morphology down to minor details (e.g., the protrusions formed in freeze-drying (Fig. 1(c))). After reduction and acid etching, the density was reduced to  $1.8\text{ mg}\cdot\text{cm}^{-3}$ , with a  $\sim 60.0\%$  weight loss. By varying the GO concentrations in aqueous dispersion through the same process, graphene aerogel with a density as low as  $1.1\text{ mg}\cdot\text{cm}^{-3}$  was obtained (Fig. S2). For comparison, a GO self-assembly was sealed in an identical ampoule without magnesium powder and directly heated to  $700\text{ }^\circ\text{C}$  with the same ramping rate. This sample was found to have broken (Fig. S3), indicating that a pyrolysis process alone may be problematic for obtaining graphene aerogels because of considerable gas release. The microstructures of the GO and rGO self-assemblies were further examined by SEM. The SEM image (Fig. S4) of the GO shows a highly interconnected, macroporous cork-like structure with a pore size of tens of micrometers. During the freezing process, GO nanosheets were expelled from the ice crystals to form a cell wall between neighboring ice crystals. After the sublimation of ice crystals, macropores were formed. TEM images of the GO (Fig. S5) self-assembly after reduction revealed that several nanometer MgO nanocrystals were dispersed on the graphene nanosheets, indicating that elemental oxygen in the GO nanosheets had combined with Mg vapor to form MgO. During the acid etching, MgO nanocrystals were removed. After freeze-drying, the rGO aerogels retained the cork-like structure (Figs. 2(a) and 2(b)) inherited from the GO assembly. Meanwhile, the



**Figure 1** Illustration of the synthesis process for graphene aerogels using magnesiothermic reaction. (a) Optical image of an aqueous GO dispersion. (b) Optical image of a freeze-dried GO self-assembly (left: top view, right: side view. Protrusions were formed during freeze-drying). (c) Optical image of rGO aerogel (left: top view, right: side view) after the magnesiothermic reduction of the GO self-assembly and subsequent acid etching and drying.



**Figure 2** SEM and TEM characterization of rGO aerogels with a density of  $1.8 \text{ mg}\cdot\text{cm}^{-3}$ . (a), (b) Low-resolution and high-resolution SEM images of rGO aerogel cross sections, respectively. (c) TEM image of rGO exhibiting few-layer morphology. (d) Electron diffraction pattern of rGO aerogel revealing its hexagonal symmetry.

walls of the rGO aerogel became nearly transparent under electron irradiation, owing to the thin and conductive nature of the nanosheets. This indicated that

the GO nanosheets were substantially reduced [27]. The high-resolution TEM image (Fig. 2(c)) of the rGO aerogels revealed that the walls of the rGO aerogels were composed of few-layer graphene sheets. Their electron diffraction pattern (Fig. 2(d)) shows hexagonal, symmetrical spots, also indicating that GO was reduced and graphenes were formed [28].

The reduction of the GO self-assembly was further confirmed by Raman, FTIR, and XPS analyses. The Raman spectra (Fig. 3(a)) of GO had a D band at  $1,350 \text{ cm}^{-1}$ , with the G band at  $1,590 \text{ cm}^{-1}$ —a ratio of 0.89. After the reduction, this ratio increased to 1.2, which can be attributed to a decrease in size of the  $\text{sp}^2$  domain (commonly observed in reduced GO [29, 30]). Figure 3(b) shows the FTIR spectra of a GO self-assembly and the rGO aerogel. The intense characteristic absorption peaks at  $3,370$ ,  $1,723$ ,  $1,223$  and  $1,048 \text{ cm}^{-1}$  were related to vibrations of the O–H, C=O, C–O–C, and C–O oxygen-containing groups, respectively [31]. After the reduction, such characteristic peaks were

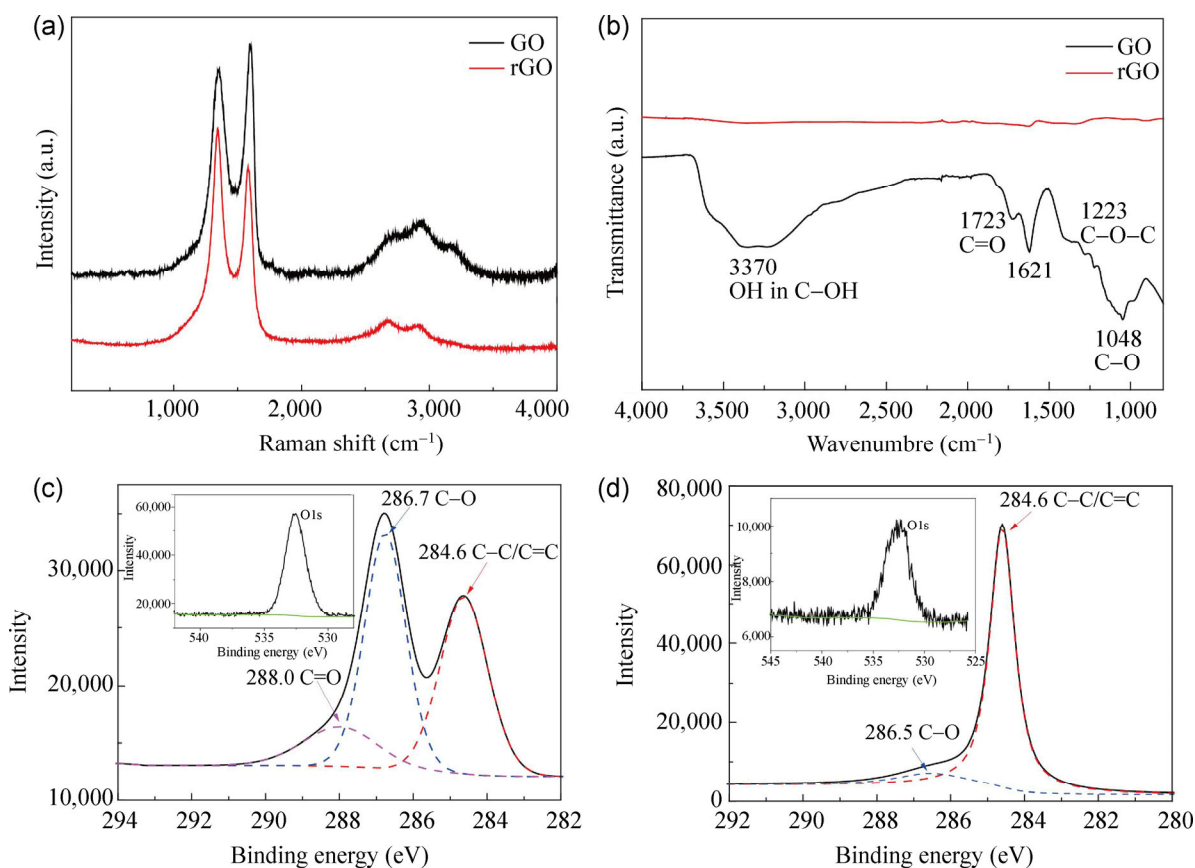


**Figure 3** Raman (a) and FTIR (b) spectra of rGO and GO, respectively. XPS spectra of GO self-assembly (c) and rGO aerogels (d), respectively.

almost completely diminished. This was consistent with the XPS analysis (Figs. 3(c) and 3(d)). Before the reduction, there were three peaks: 284.6, 286.7, and 288.0 eV, corresponding to C–C/ C=C, C–O, and C=O species, respectively [32]. After the reduction, the C=O peak disappeared and the intensity of the C–O peak was greatly reduced. The C/O atomic ratio increased from 2.0:1 before reduction to 23.4:1 after reduction (the C/O atomic ratio was calculated as the area ratio under C1s and O1s peaks multiplied by the ratio of the relative sensitivity factors of oxygen and carbon). Thus, the C/O ratio of graphene aerogels produced through magnesiothermic reaction was larger than that of most other reduced graphene aerogels (Table 1). During the reduction, the magnesium vapor reacted with the oxygen-containing groups of GO to form graphene, MgO, and possibly gaseous  $H_2/CH_x$ . In addition, the heat released in the reaction also facilitated the formation of the graphitic structures. The above results suggest that magnesiothermic reaction is an effective means for reducing GO self-assemblies into graphene aerogels.

**Table 1** Comparison of the C/O ratio of rGO aerogels via various reduction methods

Materials	Methods of reduction	C/O atomic ratio	Ref.
Self-assembled graphene hydrogel	GO self-assembly by hydrothermal Reduction	5.3	9
Graphene aerogel	GO self-assembly by L-ascorbic acid	6.4	10
Graphene sponge	GO self-assembly by hydrothermal treatment with the assistance of thiourea	11.3	14
Graphene elastomers	GO self-assembly by ascorbic acid;	6.1	17
Functionalized graphene aerogel	GO self-assembly by ethylenediamine	2.3	18
Ultralight graphene aerogel	Reduced by ethylenediamine and heating with microwaves	23	
Chemically converted graphene xerogel	GO suspension by a hypophosphorous acid–iodine	14.7	20
Macroporous graphene monoliths	Reduced by modified hydrothermal method	6.86	21
Graphene aerogel	GO self-assembly by magnesiothermic reduction	23.4	This work

Next, the elastic behavior of graphene aerogels was evaluated with quasi-static compression tests. During these tests, the aerogel samples were placed on compression plates without being glued or otherwise attached. Figure 4(a) shows the resulting stress–strain curves of rGO aerogels with a density of  $1.8 \text{ mg}\cdot\text{cm}^{-3}$  under a strain of  $\leq 50\%$  at a constant loading/unloading speed of  $2 \text{ mm}\cdot\text{min}^{-1}$  in the 1<sup>st</sup>, 2<sup>nd</sup>, 3<sup>rd</sup>, 10<sup>th</sup>, 300<sup>th</sup>, and 1,000<sup>th</sup> compression cycles. Two regimes were observed in the stress–strain curve in the loading branch of the first cycle. The linear-elastic regime ( $\varepsilon < 20\%$ ), with a modulus of 4.7 kPa, corresponded to the elastic bending of the cell walls. This value is comparable to those of graphene aerogels reinforced with carbon nanotubes with similar densities, but is higher than those of graphene elastomers reduced by ascorbic acid [13, 17]. In the non-linear regime ( $20\% < \varepsilon < 50\%$ ), the modulus increased with strain. This was related to buckling of the cell wall and densification of the cell. The stress–strain curves of consecutive compression cycles were similar. Such behavior was also observed in compression tests of nickel microlattices [33–34]. This indicates that the microstructure of the graphene aerogel became stable and recoverable after the first compression cycle. After the 1,000<sup>th</sup> cycle, the permanent deformation of the graphene aerogel was less than 4%, which was estimated from the intercept of the unloading curve with the strain axis in Fig. 4(a). Moreover, the graphene aerogel retained its macroscopic shape (inset in Fig. 4(a)). The maximum stress corresponding to 50% strain in the 1,000<sup>th</sup> cycle was only 20% lower than the stress in the first cycle. These rGO aerogels even endured strains up to 80%. When unloaded, they still recovered their original shape (Movie S1). The above results indicate an excellent elasticity of such rGO aerogels, which may be related to their microstructural resemblance to cork, which generally enables materials to be lightweight and mechanically strong. The microstructure inherited from the freeze-dried GO assembly was retained during the magnesiothermic reaction process. The appearance of hysteresis in the stress–strain curves indicated that there was energy loss in each compression cycle. The energy loss could be ascribed to the debinding process of cell walls that

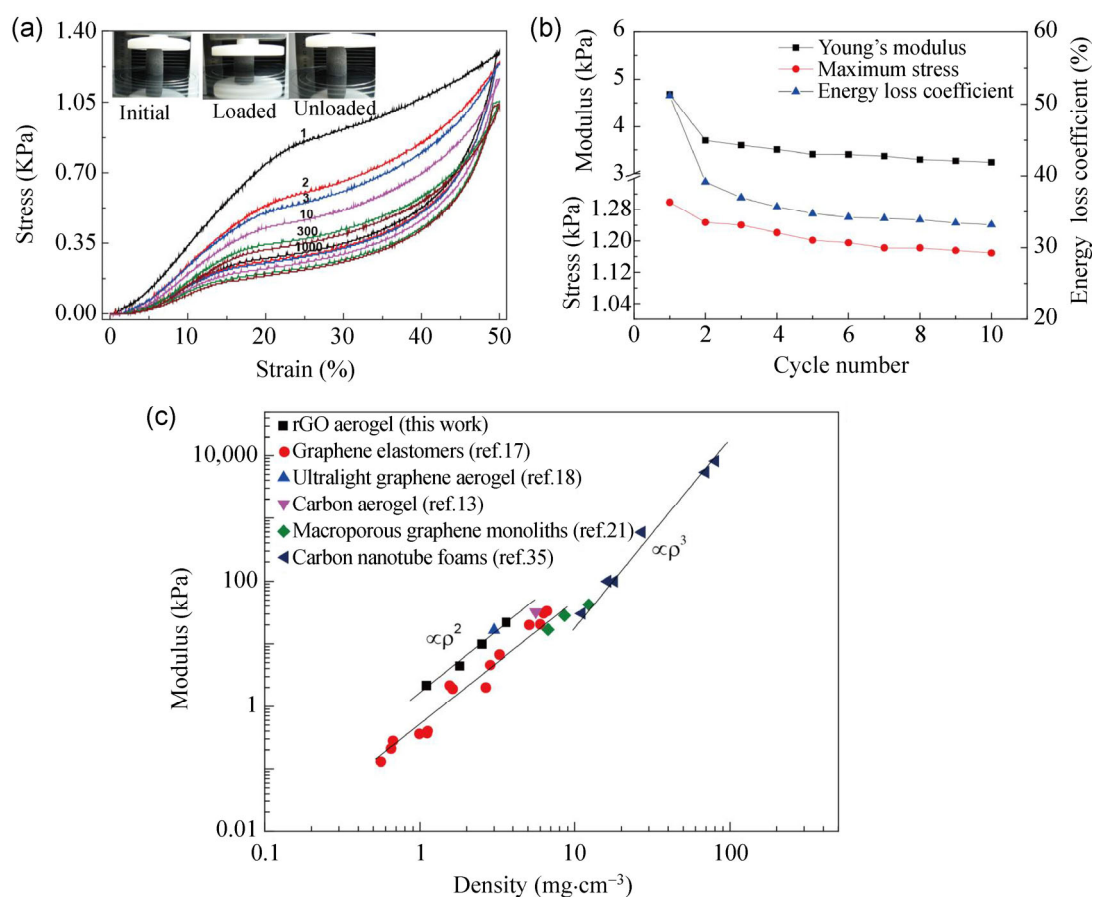


**Figure 4** Mechanical properties of rGO aerogels with a density of  $1.8 \text{ mg}\cdot\text{cm}^{-3}$  for a loading/unloading rate of  $2.0 \text{ mm}\cdot\text{min}^{-3}$ . (a) Stress–strain curves of rGO aerogel under a strain of  $\leq 50\%$  for the 1<sup>st</sup>, 2<sup>nd</sup>, 10<sup>th</sup>, 300<sup>th</sup>, and 1,000<sup>th</sup> compression cycles (inset, optical images of graphene aerogels at initial, compressed, and recovered states). (b) Young's modulus, maximum stress, and energy loss coefficient for the first ten cycles. (c) Compression modulus (modulus derived from the linear regime of the stress–strain curves) of graphene aerogels with various low densities and a comparison with other carbon-based aerogels.

had been adhered by van der Waals forces and frictions between the cell walls [17]. The extra energy loss in the first cycle (Fig. 4(b)) was due to microcracking in the graphene aerogel. In the following cycles, the microstructure of the graphene aerogels became stable and the modulus and maximum stress remained nearly constant. The modulus derived from the linear regime in the stress–strain curves of the aerogels in their first cycle is plotted against their densities in Fig. 4(c). The modulus increased when densities increased. At the higher densities, the cell walls of the graphene aerogel consisted of more layers of oriented graphene sheets (Fig. S6). Since the bending strength increased when the thickness of cell wall increased, the modulus of the aerogel increased with density. Unlike the modulus of carbon-nanotube foam (proportional to

$\rho^3$ , where  $\rho$  is density), the modulus of rGO aerogel was found to be proportional to  $\rho^2$  [35]. Such scaling indicated a bending-dominant mechanical behavior, which has been observed in nickel micro-lattices, cellular materials, and rGO aerogels reduced by ascorbic acid [17, 33, 34]. Figure 4(c) also shows an elastic modulus comparison between our graphene aerogels and graphene aerogels fabricated via other processes; our samples' elastic moduli were higher than many of the other graphene aerogels having similar densities.

Electrical conductivity was measured by a two-probe method. Figure 5(a) shows the electrical conductivities of rGO aerogels, and other reported carbon-based aerogels at various densities for comparison. The conductivity of our samples at  $3.6 \text{ mg}\cdot\text{cm}^{-3}$  was three times the value reported in a graphene elastomer with

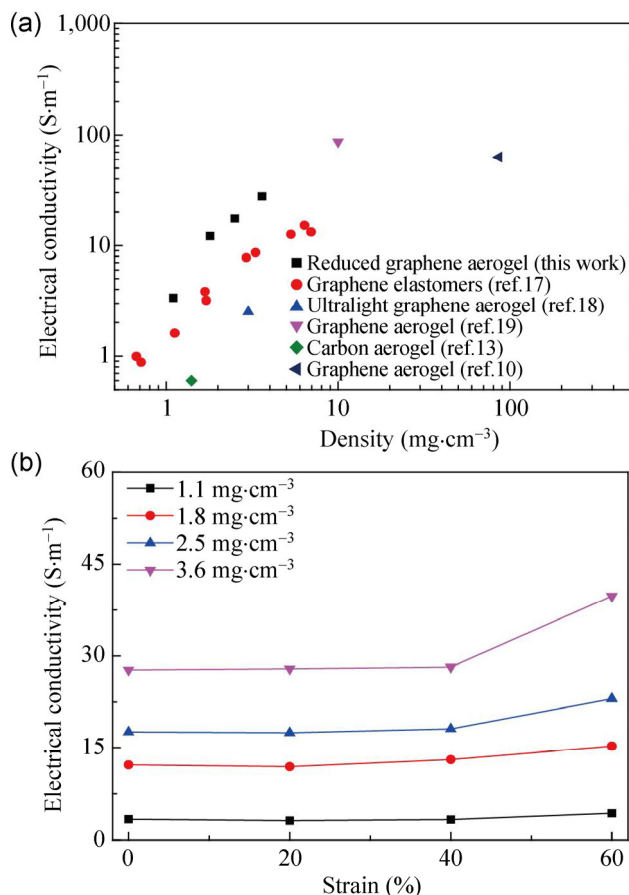


**Figure 5** (a) Electrical conductivities of rGO aerogels and other carbon-based aerogels at various densities for comparison. (b) Electrical conductivities of rGO with various densities versus strain.

a similar density that had been reduced by ascorbic acid, and superior to many graphene aerogels made using other processes [13, 17, 18]. This reinforces the assumption that GO was highly reduced by the magnesiothermic reaction. The conductivity of the rGO aerogels also changed with strain or pressure. Figure 5(b) shows the conductivity change versus strain at various densities. The conductivity changed dramatically only for strains greater than 40%. This was also ascribed to the densification and bridging of cell walls under high strain, consistent with its mechanical behavior. Such behavior might make it possible for synthesized rGO aerogels to be integrated into sensors for the detection of pressures beyond a specific threshold.

The synthesized graphene aerogels were also tested as binder-free electrodes for lithium-ion batteries. The rate capability and cycling performance of these electrodes is shown in Fig. S7. Under the specific

discharge/charge densities of 0.1, 0.2, 0.5, 1, and 2 A·g<sup>-1</sup>, the reversible current capacities were 151.3, 123.4, 98.6, 86.4, and 72.8 mAh·g<sup>-1</sup>, respectively. When the specific current was reverted to 0.5 A·g<sup>-1</sup>, these capacities increased to 131.7 mAh·g<sup>-1</sup> after 100 cycles, which might be attributed to the gradual activation of the graphene aerogel. This electrochemical performance was superior to that observed in binder-free graphene papers [36, 37].

In conclusion, highly reduced graphene oxide aerogels were successfully fabricated through the magnesiothermic reduction of freeze-dried GO self-assemblies. These rGO aerogels consisted of a highly interconnected, macroporous structure, and exhibited excellent mechanical properties as well as densities as low as 1.1 mg·cm<sup>-3</sup>. Additionally, rGO aerogel samples with densities of 1.8 mg·cm<sup>-3</sup> were fully recovered after undergoing strains of up to 80%. After a 1,000-cycle compression test, these samples retained their shape under stress levels up to 80% of that in the first cycle. Their elastic modulus scaled with density as  $E \sim \rho^2$ . These rGO aerogels also exhibited high conductivities (e.g., 27.7 S·m<sup>-1</sup> at 3.6 mg·cm<sup>-3</sup>) and outperformed many rGO aerogels fabricated by other processes. Thus, the magnesiothermic reduction process, together with freeze-drying process, creates a robust, open macroporous microstructure with relatively high conductivity. This, in turn, makes rGO aerogels promising for many applications such as catalysis supports, pressure-sensors, and electrode materials.

## Acknowledgements

This work was supported by the Scientific Research Foundation for Returned Scholars, the Ministry of Education of China, Key Basic Research Projects of Science and Technology Commission of Shanghai (No. 11JC1412900), and the National Science Foundation of China program (Nos. 21271140, 51472182).

**Electronic Supplementary Material:** Supplementary material (details of the synthesis of the graphene aerogel, mechanical and conductivity testing, electrochemical measurements, and additional experimental images) is available in the online version of this article at <http://dx.doi.org/10.1007/s12274-014-0672-z>.

## References

- [1] Novoselov, K. S.; Geim, A. K.; Morozov, S. V.; Jiang, D.; Zhang, Y.; Dubonos, S. V.; Grigorieva, I. V.; Firsov, A. A. Electric field effect in atomically thin carbon films. *Science* **2004**, *306*, 666–669.
- [2] Ferrari, A. C.; Meyer, J. C.; Scardaci, V.; Casiraghi, C.; Lazzeri, M.; Mauri, F.; Piscanec, S.; Jiang, D.; Novoselov, K. S.; Roth, S. et al. Raman spectrum of graphene and graphene layers. *Phys. Rev. Lett.* **2006**, *97*, 187401.
- [3] Geim, A. K. Graphene: Status and prospects. *science* **2009**, *324*, 1530–1534.
- [4] Lee, C.; Wei, X. D.; Kysar, J. W.; Hone, J. Measurement of the elastic properties and intrinsic strength of monolayer graphene. *Science* **2008**, *321*, 385–388.
- [5] Balandin, A. A.; Ghosh, S.; Bao, W. Z.; Calizo, I.; Teweldebrhan, D.; Miao, F.; Lau, C. N. Superior thermal conductivity of single-layer graphene. *Nano Lett.* **2008**, *8*, 902–907.
- [6] Zhu, Y. W.; Murali, S.; Stoller, M. D.; Ganesh, K. J.; Cai, W. W.; Ferreira, P. J.; Pirkle, A.; Wallace, R. M.; Cychosz, K. A.; Thommes, M. et al. Carbon-based supercapacitors produced by activation of graphene. *Science* **2011**, *332*, 1537–1541.
- [7] Novoselov, K. S.; Fal'ko, V. I.; Colombo, L.; Gellert, P. R.; Schwab, M. G.; Kim, K. A roadmap for graphene. *Nature* **2012**, *490*, 192–200.
- [8] Orlita, M.; Faugeras, C.; Plochocka, P.; Neugebauer, P.; Martinez, G.; Maude, D. K.; Barra, A. L.; Sprinkle, M.; Berger, C.; de Heer, W. A. et al. Approaching the dirac point in high-mobility multilayer epitaxial graphene. *Phys. Rev. Lett.* **2008**, *101*, 267601.
- [9] Xu, Y. X.; Sheng, K. X.; Li, C.; Shi, G. Q. Self-assembled graphene hydrogel via a one-step hydrothermal process. *ACS Nano* **2010**, *4*, 4324–4330.
- [10] Zhang, X. T.; Sui, Z. Y.; Xu, B.; Yue, S. F.; Luo, Y. J.; Zhan, W. C.; Liu, B. Mechanically strong and highly conductive graphene aerogel and its use as electrodes for electrochemical power sources. *J. Mater. Chem.* **2011**, *21*, 6494–6497.
- [11] Wu, Z.-S.; Yang, S. B.; Sun, Y.; Parvez, K.; Feng, X. L.; Muellen, K. 3D nitrogen-doped graphene aerogel-supported Fe<sub>3</sub>O<sub>4</sub> nanoparticles as efficient electrocatalysts for the oxygen reduction reaction. *J. Am. Chem. Soc.* **2012**, *134*, 9082–9085.
- [12] Zhao, Y.; Hu, C. G.; Hu, Y.; Cheng, H. H.; Shi, G. Q.; Qu, L. T. A versatile, ultralight, nitrogen-doped graphene framework. *Angew. Chem. Int. Ed.* **2012**, *51*, 11371–11375.
- [13] Sun, H. Y.; Xu, Z.; Gao, C. Multifunctional, ultra-flyweight, synergistically assembled carbon aerogels. *Adv. Mater.* **2013**, *25*, 2554–2560.
- [14] Zhao, J. P.; Ren, W. C.; Cheng, H.-M. Graphene sponge for efficient and repeatable adsorption and desorption of water contaminations. *J. Mater. Chem.* **2012**, *22*, 20197–20202.
- [15] Nardecchia, S.; Carriazo, D.; Ferrer, M. L.; Gutiérrez, M. C.; del Monte, F. Three dimensional macroporous architectures and aerogels built of carbon nanotubes and/or graphene: Synthesis and applications. *Chem. Soc. Rev.* **2013**, *42*, 794–830.
- [16] Chabot, V.; Higgins, D.; Yu, A. P.; Xiao, X. C.; Chen, Z. W.; Zhang, J. J. A review of graphene and graphene oxide sponge: Material synthesis and applications to energy and the environment. *Energy Environ. Sci.* **2014**, *7*, 1564–1596.
- [17] Qiu, L.; Liu, J. Z.; Chang, S. L. Y.; Wu, Y. Z.; Li, D. Biomimetic superelastic graphene-based cellular monoliths. *Nat. Commun.* **2012**, *3*, 1241.
- [18] Hu, H.; Zhao, Z. B.; Wan, W. B.; Gogotsi, Y.; Qiu, J. S. Ultralight and highly compressible graphene aerogels. *Adv. Mater.* **2013**, *25*, 2219–2223.
- [19] Worsley, M. A.; Pauzaskie, P. J.; Olson, T. Y.; Biener, J.; Satcher, J. H.; Baumann, T. F. Synthesis of graphene aerogel with high electrical conductivity. *J. Am. Chem. Soc.* **2010**, *132*, 14067–14069.
- [20] Pham, H. D.; Pham, V. H.; Cuong, T. V.; Nguyen-Phan, T. D.; Chung, J. S.; Shin, E. W.; Kim, S. Synthesis of the chemically converted graphene xerogel with superior electrical conductivity. *Chem. Commun.* **2011**, *47*, 9672–9674.
- [21] Li, Y. R.; Chen, J.; Huang, L.; Li, C.; Hong, J.-D.; Shi, G. Q. Highly compressible macroporous graphene monoliths via an improved hydrothermal process. *Adv. Mater.* **2014**, *26*, 4789–4793.
- [22] Lin, Y. R.; Ehlert, G. J.; Bukowsky, C.; Sodano, H. A. Superhydrophobic functionalized graphene aerogels. *ACS Appl. Mater. Interfaces* **2011**, *3*, 2200–2203.
- [23] Bao, Z. H.; Weatherspoon, M. R.; Shian, S.; Cai, Y.; Graham, P. D.; Allan, S. M.; Ahmad, G.; Dickerson, M. B.; Church, B. C.; Kang, Z. T. Chemical reduction of three-dimensional silica micro-assemblies into microporous silicon replicas. *Nature* **2007**, *446*, 172–175.
- [24] Xing, A.; Zhang, J.; Bao, Z. H.; Mei, Y. F.; Gordin, A. S.; Sandhage, K. H. A magnesiothermic reaction process for the scalable production of mesoporous silicon for rechargeable lithium batteries. *Chem. Commun.* **2013**, *49*, 6743–6745.
- [25] Hummers, W. S.; Offeman, R. E. Preparation of graphitic oxide. *J. Am. Chem. Soc.* **1958**, *80*, 1339–1339.
- [26] Cote, L. J.; Kim, F.; Huang, J. X. Langmuir-blodgett assembly of graphite oxide single layers. *J. Am. Chem. Soc.* **2009**, *131*, 1043–1049.
- [27] Eda, G.; Fanchini, G.; Chhowalla, M. Large-area ultrathin films of reduced graphene oxide as a transparent and flexible electronic material. *Nat. Nanotechnol.* **2008**, *3*, 270–274.

- [28] Warner, J. H.; Rummeli, M. H.; Gemming, T.; Büchner, B.; Briggs, G. A. D. Direct imaging of rotational stacking faults in few layer graphene. *Nano Lett.* **2009**, *9*, 102–106.
- [29] Nguyen, S. T.; Ruoff, R. S.; Stankovich, S.; Dikin, D. A.; Piner, R. D.; Kohlhaas, K. A.; Kleinhammes, A.; Jia, Y. Y.; Wu, Y. Synthesis of graphene-based nanosheets via chemical reduction of exfoliated graphite oxide. *Carbon* **2007**, *45*, 1558–1565.
- [30] Kudin, K. N.; Ozbas, B.; Schniepp, H. C.; Prud'homme, R. K.; Aksay, I. A.; Car, R. Raman spectra of graphite oxide and functionalized graphene sheets. *Nano Lett.* **2008**, *8*, 36–41.
- [31] Liu, H. T.; Zhang, L.; Guo, Y. L.; Cheng, C.; Yang, L. J.; Jiang, L.; Yu, G.; Hu, W. P.; Liu, Y. G.; Zhu, D. B. Reduction of graphene oxide to highly conductive graphene by lawesson's reagent and its electrical applications. *J. Mater. Chem. C* **2013**, *1*, 3104–3109.
- [32] Fernandez-Merino, M. J.; Guardia, L.; Paredes, J. I.; Villar-Rodil, S.; Solis-Fernandez, P.; Martinez-Alonso, A.; Tascon, J. M. D. Vitamin C is an ideal substitute for hydrazine in the reduction of graphene oxide suspensions. *J. Phys. Chem. C* **2010**, *114*, 6426–6432.
- [33] Salari-Sharif, L.; Schaedler, T. A.; Valdevit, L. Energy dissipation mechanisms in hollow metallic microlattices. *J. Mater. Res.* **2014**, *29*, 1755–1770.
- [34] Schaedler, T. A.; Jacobsen, A. J.; Torrents, A.; Sorensen, A. E.; Lian, J.; Greer, J. R.; Valdevit, L.; Carter, W. B. Ultralight metallic microlattices. *Science* **2011**, *334*, 962–965.
- [35] Worsley, M. A.; Kucheyev, S. O.; Satcher, J. H.; Hamza, A. V.; Baumann, T. F. Mechanically robust and electrically conductive carbon nanotube foams. *Appl. Phys. Lett.* **2009**, *94*, 073115.
- [36] Liu, S. Y.; Chen, K.; Fu, Y.; Yu, S. Y.; Bao, Z. H. Reduced graphene oxide paper by supercritical ethanol treatment and its electrochemical properties. *Appl. Sur. Sci.* **2012**, *258*, 5299–5303.
- [37] Abouimrane, A.; Compton, O. C.; Amine, K.; Nguyen, S. T. Non-annealed graphene paper as a binder-free anode for lithium-ion batteries. *J. Phys. Chem. C* **2010**, *114*, 12800–12804.